Int. J. Electrochem. Sci., 17 **(2022)** Article Number: 220139, doi: 10.20964/2022.01.25

International Journal of
ELECTROCHEMICAL
SCIENCE
www.electrochemsci.org

Investigation of Erosion-corrosion of Carbon Steel Elbow in 3.5% Sodium Chloride Containing Quartz

Zongwu Hu[1,*], *Rui Xing*[2], *Jianguo Liu*[3]

[1] Lanzhou University of Technology, Lanzhou 730050, China
[2] Lanzhou Testing Technology Co. Ltd. of Chinese Academy of Inspection and Quarantine, Lanzhou 730070, China
[3] China University of Petroleum (East China), Qingdao 266580, China
[*]E-mail: huzongwu587@163.com

Received: 23 September 2021 / *Accepted:* 25 October 2021 / *Published:* 6 December 2021

In this study, the erosion-corrosion (E-C) behavior at different locations of a 90° horizontal elbow was investigated under the condition of liquid-solid two-phase flow by weight loss measurement, electrochemical measurement and surface analysis through a loop experimental device. Besides, a quantitative analysis was performed on the pure corrosion rate, the pure erosion rate, the changed amount of corrosion rate caused by erosion, and the changed amount of erosion rate caused by corrosion and their percentages in the E-C rate, in an attempt to reveal the damage mechanism of metal materials. There were different E-C rates, electrochemical characteristics and surface morphologies at different locations of the elbow; the areas with severe E-C appeared at the bottom of the elbow and the outer part of the elbow outlet; surface morphologies were mainly presented as pits and grooves. In the total E-C rates, the percentages of pure corrosion rates and pure erosion rates were very small, while that of E-C interaction rates were large, which demonstrated that the interaction between electrochemical corrosion and mechanical erosion was the main cause of damage to metal materials. In the E-C process, mechanical erosion and electrochemical corrosion can contribute to each other, with the former playing a dominant role and the latter playing a subordinate role.

Keywords: Liquid-solid flow; 90° horizontal elbow; erosion-corrosion; interaction

1. INTRODUCTION

Under flowing conditions, there is relative motion between the metal surface and corrosive medium, namely E-C, which could cause a significant increase in the corrosion rate of metal [1, 2]. The metal damage in the E-C environment is not a simple combination of electrochemical corrosion and mechanical erosion processes, but a result of the interaction between electrochemical corrosion and mechanical erosion processes [3-5]. E-C refers to a kind of local corrosion with serious hazards

[6]. In the oil and gas storage and transportation system, E-C occurs extensively in metal pipelines and equipment, and it is more serious in the oil and gas gathering and transportation network [7]. Besides, E-C is prone to occur due to the fact that there are often multiphase flowing media, such as liquid/solid or gas/liquid/solid, in the gathering and transportation network, which greatly intensifies corrosion. In the gathering and transportation network, the mechanical equipment (such as elbows, tees and valves) suffers from severe E-C, which decreases the wall thickness of equipment rapidly [8, 9]. As a result, the service life is greatly shortened [10], and serious safety accidents may even be induced, which not only affects the normal production of enterprises, but also causes heavy casualties and economic losses.

The E-C of metal materials in liquid/solid two-phase flow is a multi-disciplinary and complex problem involving electrochemistry, materials science and hydrodynamics [11, 12]. At present, researchers have conducted many studies on the E-C process of metal materials, and obtained a certain understanding of the composition of E-C process. Stack et al. [13, 14] conducted a thorough investigation on the E-C process of metals and demonstrated that the loss of metal in E-C process is mainly composed of four components, namely the pure erosion, pure corrosion, changed amount of corrosion rate caused by erosion, and changed amount of erosion rate caused by corrosion. However, there are some disputes about the interaction mechanism between erosion and corrosion. Yang et al. [12] made an exploration on the erosion-corrosion process through some experiments, and they suggested that mechanical erosion plays a dominant role in the erosion-corrosion process. However, Malka Ramakrishna et al. [15] also studied the erosion-corrosion process through some experiments, and found that electrochemical corrosion played a major role in the erosion-corrosion process.

Currently, numerical simulation has been adopted extensively to investigate the E-C process of metals [16-18]. However, this method can only be used to simulate the erosion process, but cannot be used to establish an accurate mathematical model for the E-C process. Hence, the interaction mechanism between mechanical erosion and electrochemical corrosion cannot be revealed by this method. In addition, there are also some studies exploring the E-C process through experiments [19-21]. Although the rotating disk (column) electrode device [22, 23] and jet device [24, 25] are the most common tools in these studies, they are quite different from the actual engineering conditions of the pipelines [26]. Further, the loop experimental device is very close to actual conditions, but it is limited by technology and detection means, and hence it is seldom applied. In oil and gas gathering and transportation systems, elbows are prone to be damaged. However, there are few experimental studies on the E-C process at different locations of elbow. Therefore, it is necessary to investigate the E-C of elbows under the condition of liquid/solid two-phase flow, so as to reveal the interaction mechanism between erosion and corrosion.

In this paper, the E-C characteristics at different locations of a 90° horizontal elbow were characterized by weight loss measurement, in situ electrochemical measurement and surface analysis through a loop experimental device designed independently. The damage mechanism of metal under the interaction between electrochemical corrosion and mechanical erosion was consequently revealed, which provides guidance for the protection of elbow against E-C and is significant to ensure the safe operation of mechanical equipment in the E-C environment.

2. EXPERIMENTAL

2.1 Experimental device

A loop experimental device was adopted in the experiments, as shown in Fig. 1. This device consists of a test elbow, a tank, a centrifugal pump, a temperature control system, a reservoir, a flow meter, a pressure gauge, and pipes. The inner diameter of the pipe is 50mm. A self-designed detachable 90° test elbow which includes the inner and outer parts is provided with 42 grooves on the inner wall of the elbow to install 42 specimens, through which E-C can be measured at different locations of the elbow, as shown in Fig. 2. The curvature radius of the elbow is equal to 1.5*D*, where *D* represents the inner diameter of pipes. In order to facilitate analysis, 42 specimens at different annular and axial angles are numbered with the code AB, as shown in Fig. 3, where A represents the No. of the axial angle θ , which are 0°, 15°, 30°, 45°, 60°, 75° and 90°, respectively, and represented by 1, 2, 3, 4, 5, 6 and 7; B represents the No. of the annular angle φ, which are 45°, 90°, 135°, 180°, 225°, 270° and 315°, respectively, and represented by 1, 2, 3, 4, 5 and 6. For example, 45 represents that the specimen is located at θ=45° and φ=270°. The outer part corresponds to annular angles φ=45°, 90° and 135°, while the inner one corresponds to annular angles φ=225°, 270° and 315°. Due to the fact that there are 42 specimens on the elbow, the specimens (No. 41, 42, 43, 44, 45, and 46) at axial angle θ=45° of the elbow are taken as the representatives for the subsequent analysis in this paper. In addition, In order to realize in-situ electrochemical measurements, an electrochemical measurement system was set at the elbow, in which the specimens were regarded as working electrodes (WE), a saturated calomel electrode (SCE) was regarded as the reference electrode and a platinum plate as the counter electrode at the elbow.

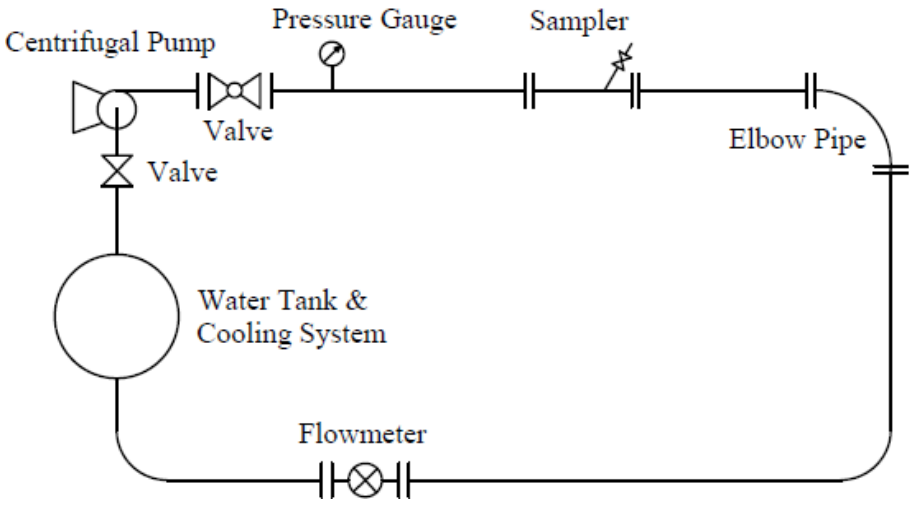

Figure 1. Schematic diagram of the loop experimental device

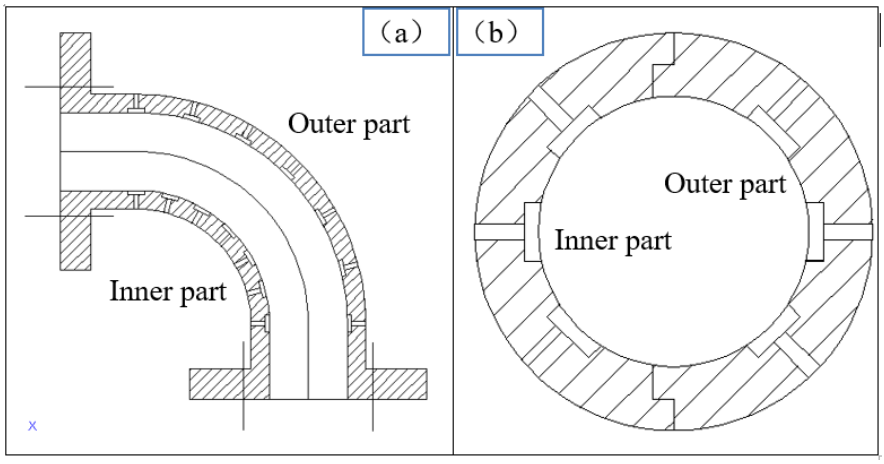

Figure 2. Cutaway view of the test elbow: (a) transverse cutaway view; (b) longitudinal cutaway view

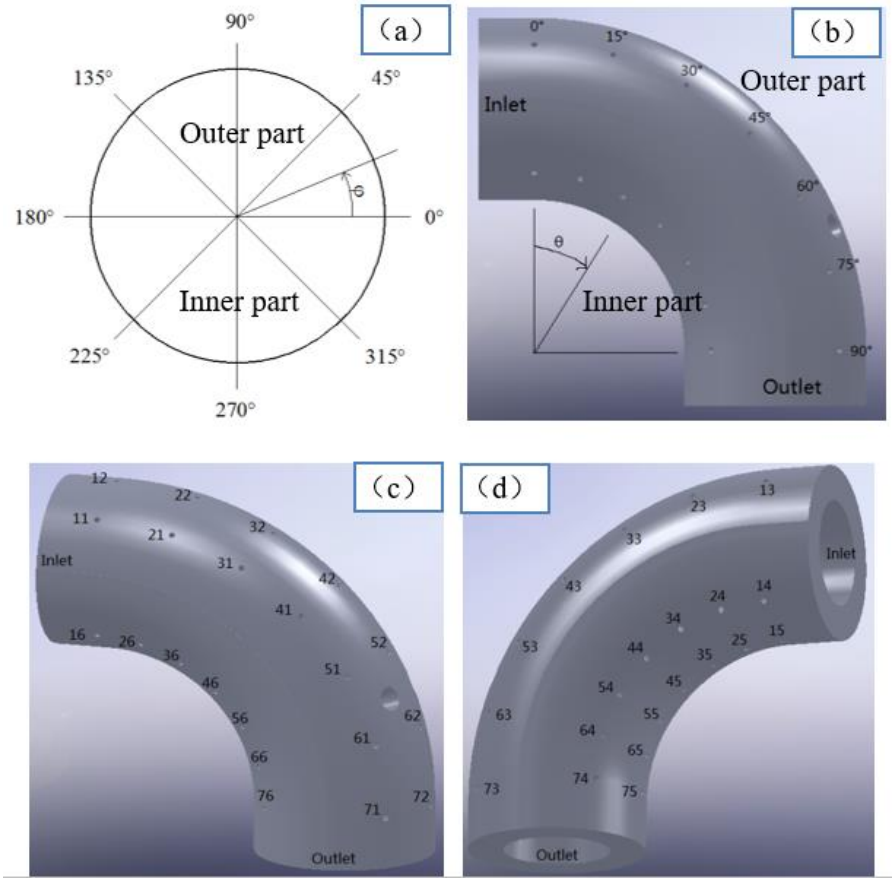

Figure 3. Schematic diagram of angles and specimen No., (a) annular angle φ, (b) axial angle θ, (c) and (d) specimen No. at the elbow

2.2 Experimental conditions

The experimental medium was 3.5 wt% NaCl solution, in which the concentration of quartz sand (60-70 mesh) was 1.25 wt%. Before being added to the solution, the quartz sand was heated in

boiling water, then rinsed with hydrochloric acid and deionized water, and dried. The temperature was maintained at 25°C, the pressure was the normal pressure, and the medium velocity was 2.5m/s. All experiments were performed within 36h, and were repeated three times. After each experiment, the solution and quartz sand were changed.

Carbon steel (20#) specimens with a size of 7.0mm×7.0mm×3.0mm and each exposed area of 0.49cm^2 were used in these experiments. The chemical composition is shown in Table 1. Before experiments, the working surfaces of specimens were wet ground to 1000 grade with silicon carbide papers, then rinsed with deionized water, degreased with acetone, dehydrated with absolute ethanol, and finally dried in a vacuum dryer for at least 24h.

Table 1. Chemical composition of 20# carbon steel

C	Si	Mn	Cr	Ni	Cu	P	S	Fe
0.19	0.28	0.52	0.25	0.3	0.25	0.035	0.035	balance

2.3 Experimental methods

In order to reveal the interaction mechanism between erosion and corrosion, these four components of E-C are quantified as follows:

$$V_T = V_{C0} + V_{E0} + \Delta V_C + \Delta V_E \quad (1)$$

$$\Delta V_S = \Delta V_C + \Delta V_E \quad (2)$$

$$V_C = V_{C0} + \Delta V_C \quad (3)$$

$$V_E = V_{E0} + \Delta V_E \quad (4)$$

where, V_T represents the total E-C rate determined by weight loss measurements; V_{C0} represents the pure corrosion rate obtained by weight loss measurements under static condition; V_{E0} represents the pure erosion rate determined by weight loss measurements after E-C experiment under the condition of cathodic protection; V_C represents the total corrosion rate determined by electrochemical impedance spectroscopy(EIS) measurements during E–C experiment; ΔV_S represents the interaction rate of E-C; V_E represents the total erosion rate obtained by V_T-V_C; ΔV_C represents the changed amount of corrosion rate caused by erosion obtained by V_C-V_{C0}; ΔV_E represents the changed amount of erosion rate caused by corrosion obtained by V_S-V_C.

2.4 Experimental measurements

Before the E-C experiment, an electronic balance was adopted to measure the qualities of specimens, and a vernier caliper was adopted to measure the sizes of specimens. One test wire was soldered on the back of each specimen. Then, 42 specimens, the reference electrode and counter electrode were mounted into the grooves of the elbow one by one with silica gel, as shown in Fig. 4. Subsequently, the inner and outer parts of the elbow were assembled. Finally, the elbow was placed for 24h to ensure stable adhesion. During the experiment, the electrochemical impedance spectrum (EIS)

measurements of 42 specimens were performed one by one. In order to shorten the measurement time and improve the measurement accuracy, EIS measurements were conducted under open circuit potential (OCP) with a frequency ranging from 100000Hz to 0.1Hz. The number of scanned points was 30, the amplitude of the AC sinusoidal excitation signal was 10mV, and the measurement time of 42 specimens in this experiment was about 1h. After this experiment, the surface macroscopic morphologies of 42 specimens were observed with a stereo microscope, and then the silica gel and corrosion products on the surface of specimens were removed. Subsequently, these specimens were washed with deionized water repeatedly, dehydrated with alcohol, and dried for 24h. Finally, they were weighed one by one. Moreover, the three-dimensional (3D) corrosion morphologies of 42 specimens were observed and the maximum groove depths on the surface of these specimens were measured with a Zeiss Axio Imager A2m 3D confocal microscope.

The potentiodynamic polarization test was conducted in 3.5wt% NaCl solution under the static condition of 25°C and atmospheric pressure, with a scan rate of 0.333mV/s and a voltage ranging from -250 to 250mV relative to open circuit potential (OCP).

To determine the pure erosion rate, an erosion experiment was performed under cathodic protection of -0.85V vs. SCE. No electrochemical measurement was required during the erosion experiment, and other conditions were exactly the same as the E-C experiment.

To determine the pure corrosion rate, a pure corrosion experiment was performed under a static condition. Prior to this experiment, one surface of the specimen was stuck to the bottom of a beaker with silica gel, so as to ensure that the other five surfaces were immersed in 3.5wt% NaCl solution. During this experiment, the beaker was placed in the water bath with a constant temperature to ensure that the solution temperature can be maintained at 25°C.

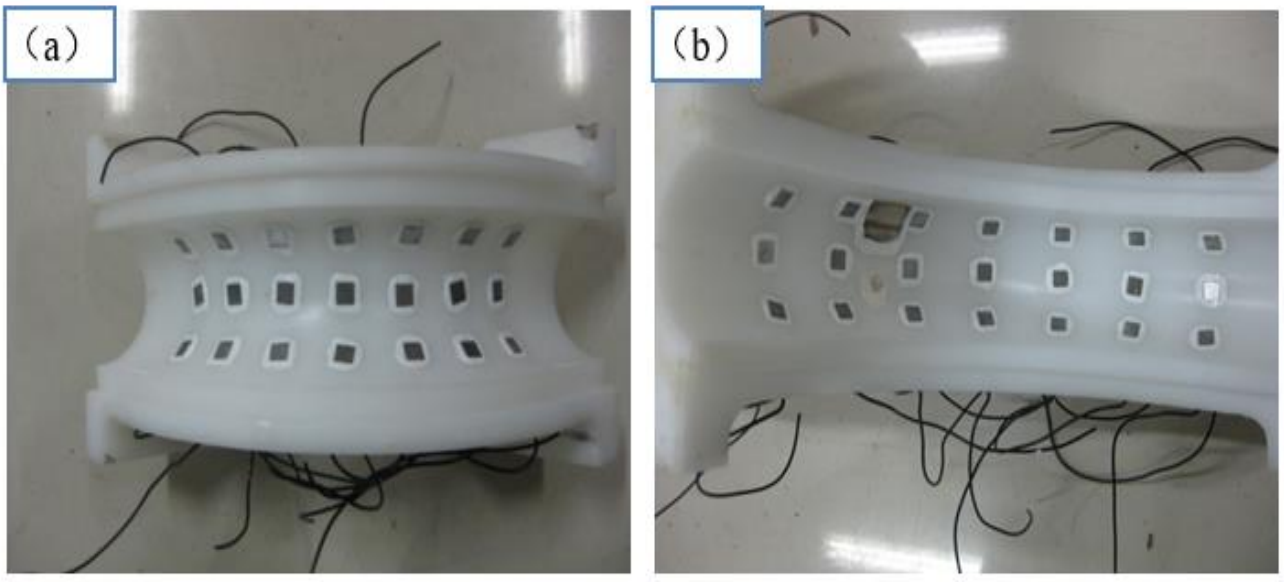

Figure 4. Physical diagram of test elbow after sealing specimens: (a) inner part and (b) outer part

3. RESULTS AND DISCUSSION

3.1 Electrochemical measurements

Fig. 5 presents the Nyquist plots of specimens at the axial angle θ=45° of the elbow. It can be seen that the Nyquist plots of specimens at the axial angle θ=45° of the elbow are similar, and they all show the characteristics of capacitive reactance arc. However, there are differences in the capacitive arc radii of specimens at different locations, which indicates different corrosion rates at different locations of the elbow. The smaller the capacitive arc radius of the specimen, the greater the corrosion rate. In order to analyze the parameters of EIS, the EIS data of 42 specimens were fitted. The EIS behavior of specimens under the condition of liquid/solid two-phase flow was analyzed by taking the average value of three experimental data fitted as the EIS parameters.

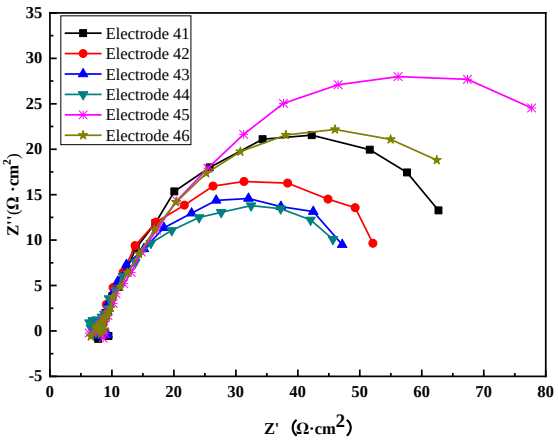

Figure 5. Nyquist plots of specimens at the axial angle θ=45° of the elbow

To obtain the charge transfer resistance and calculate the total corrosion rate, EIS data of 42 specimens were fitted by ZSimpWin software with an electrochemical equivalent circuit. As shown in Fig. 6, R_s represents the solution resistance, CPE1 represents the constant phase element, R_f represents the corrosion product film resistance, CPE2 represents the constant phase angle element of double electric layer between metal matrix and solution, and R_t represents the charge transfer resistance. The values of the corresponding fitted impedance parameters of typical specimens (No. 41, 42, 43, 44, 45, and 46) are listed in Table 2. It can be seen that the fitting effect is favorable. The higher the corrosion resistance, the lower the corrosion rate. As presented in this table, the charge transfer resistance of specimen 42 is smaller than that of specimen 45, and hence the corrosion rate of specimen 42 is greater than that of specimen 45, which is completely consistent with the result of weight loss measurement.

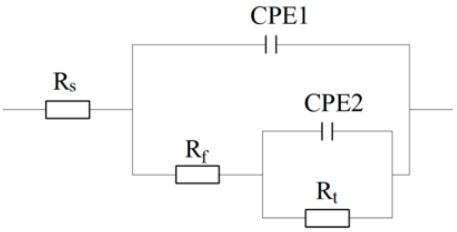

Figure 6. Electrochemical equivalent circuit for EIS fitting

Table 2. Fitted parameters of EIS of typical specimens

Specimens NO	R_s ($\Omega\cdot cm^2$)	CPE1-Y_0 ($\Omega\cdot cm^{-2}\cdot s^{-1}$)	CPE1-n_1 —	R_f ($\Omega\cdot cm^2$)	CPE2-Y_0 ($\Omega\cdot cm^{-2}\cdot s^{-1}$)	CPE2-n_2 —	R_t ($\Omega\cdot cm^2$)
41	8.436	0.001373	0.8329	4.021	0.004546	0.7509	92.06
42	7.921	0.005899	0.6589	12.05	0.001094	1	78.01
43	7.917	0.00517	0.6467	7.258	0.001655	0.8518	71.43
44	7.794	0.004898	0.7051	11.24	0.005674	0.6785	74.59
45	8.098	0.002465	0.939	3.470	0.05152	0.6591	111.5
46	8.002	0.005844	0.5783	13.5	0.003939	0.6128	112.2

Fig. 7 presents the polarization curve of specimen. The processes of anode and cathode are fitted and the fitting results are listed in Table 3. The total corrosion current density in this study is calculated according to Stern-Geary equation (5) [27], so that the total corrosion rate V_C can be calculated. Fig. 8 presents the total corrosion rates at different locations of the elbow.

$$i_{corr} = \frac{B_a \times B_c}{2.303\left(B_a + B_c\right)} \times \frac{1}{R_t} = \frac{B}{R_t} \qquad (5)$$

where, B represents the Stern-Geary coefficient of the Tafel curve, B_a represents the Tafel slope of the anode, B_c represents the Tafel slope of the cathode, and R_t represents the charge transfer resistance obtained by EIS fitted.

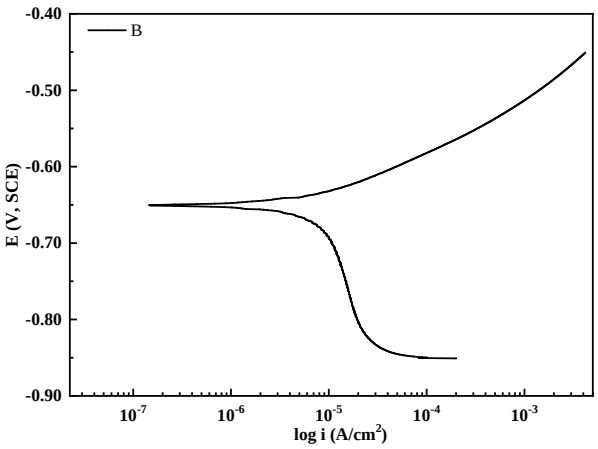

Figure 7. Polarization curve of specimens in 3.5wt% NaCl solution

Table 3. Fitting parameters of polarization curve

Parameter Name	E_{corr}(mV)	I_{corr}(μA/cm^2)	B_a(mV)	B_c(mV)
Value	650	5.5	71	824

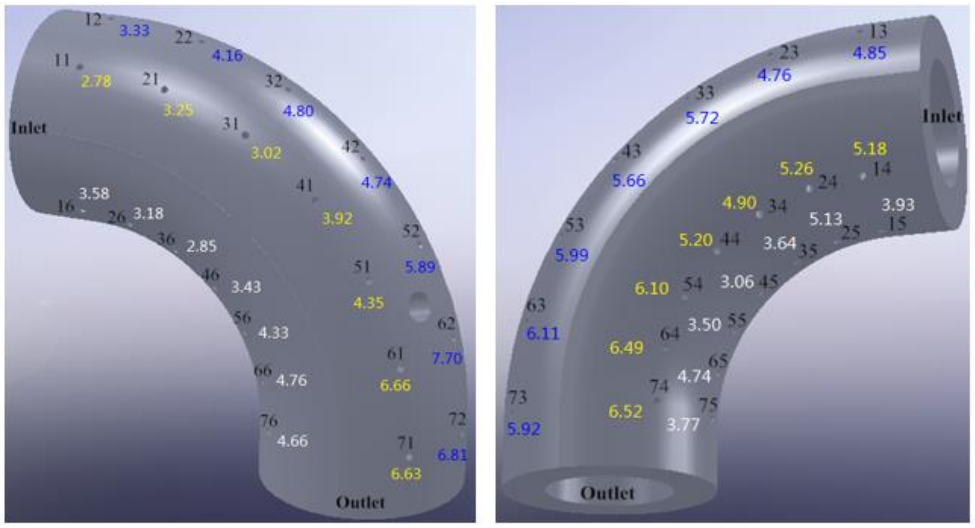

Figure 8. Total corrosion rates at different locations of the elbow

3.2 E-C rates

3.2.1 Total E-C rates

Fig. 9 presents the total E-C rates at different locations of the elbow. It can be seen that there are different total E-C rates at different locations of the elbow (between 3.49 and 8.81mm/yr). The areas with severe E-C appear at the bottom of the elbow (annular angle φ=135° and 225°) and the outer part of the elbow outlet (axial angle θ=60°, 75° and 90°). On the ground that the concentration of quartz sand at the bottom of the elbow is higher [28], the surfaces of specimens are scoured and sheared more strongly by the medium, which induces higher total E-C rates. At the outer part of the elbow outlet, a secondary flow phenomenon is formed [14] due to the fact that the medium is affected by the geometric shape of the elbow. Therefore, the outer part of the elbow outlet is subjected to stronger scouring and shearing action of the liquid/solid two-phase flowing medium [29], resulting in an increase in the E-C rate and more serious damage to materials. Peng et al. [30] studied the sand particle erosion under the slug flow condition in a horizontal pipe bend by experiment and numerical simulation. The results of this study are similar to the findings of their study.

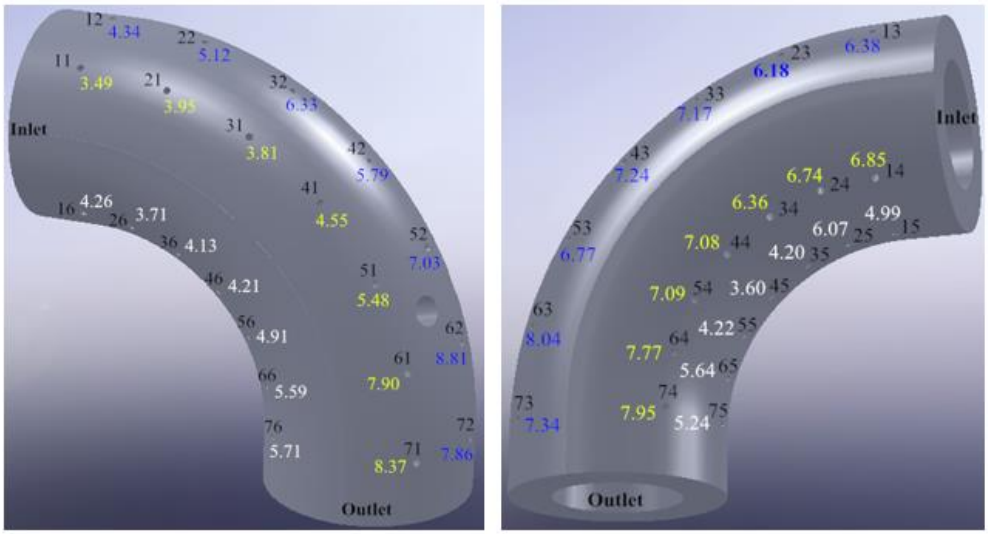

Figure 9. Total E-C rates at different locations of the elbow

3.2.2 Pure corrosion rate

The pure corrosion rate at different locations of the elbow is the same for the reason that it is measured under the static conditions. The pure corrosion rate is 0.24mm/yr, which is very small. Besides, its percentage in the E-C rate is also small, between 2.7% and 6.9%. It can be seen that the E-C rates are much higher than the pure corrosion rates at different locations of the elbow. The reason is that under the condition of liquid/solid two-phase flow, the surfaces of the specimens are subjected to strong mechanical erosion, which causes the continuous falling of corrosion products. Besides, the new metal substrate is exposed in the corrosive medium, which causes continuous dissolving of the metal dissolve, thereby promoting the corrosion process [31, 32]. Meanwhile, the flow of medium improves the oxygen diffusion coefficient and charge transfer rate. Besides, depolarization promotes the reaction of cathode and anode during the electrochemical corrosion, and accelerates the corrosion process, which induces a significant increase in the E-C rate. Therefore, the mechanical erosion of medium promotes the E-C process under liquid/solid two-phase flow conditions.

3.2.3 Pure erosion rates

Fig. 10 presents the pure erosion rates at different locations of the elbow. It can be seen that the pure erosion rates are small, between 0.06 and 0.31mm/yr, and their percentages in the E-C rate are also small, between 0.9% and 4.7%. Therefore, electrochemical corrosion could also promote the E-C process.

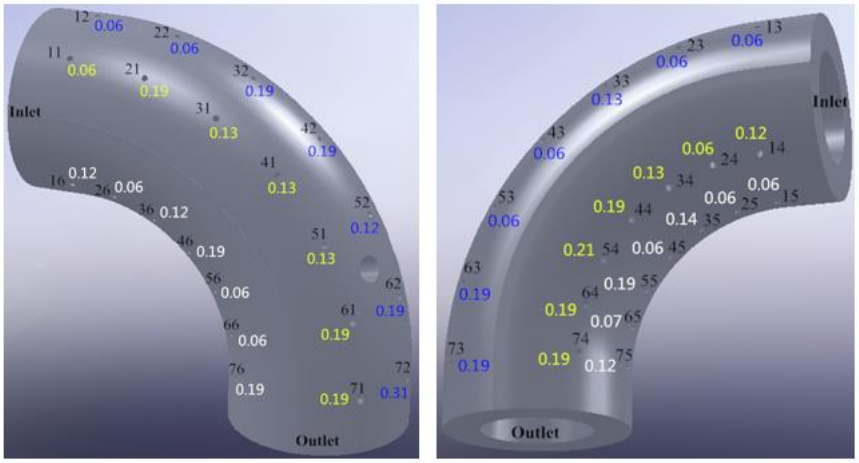

Figure 10. Pure erosion rates at different locations of the elbow

3.2.4 E-C interaction rates

Fig. 11 presents the E-C interaction rates at different locations of the elbow. It can be seen that the E-C interaction rates are large, between 3.19 and 8.38 mm/yr. Their percentages in the E-C rates are also very high, between 89.2% and 95.8%. Therefore, the interaction between mechanical erosion and electrochemical corrosion under the condition of liquid/solid two-phase flow is the dominant cause of metal damage, the metal weight loss caused by the interaction between erosion and corrosion can be selected as a measure of E-C weight loss. This is consistent with the conclusions of Zeng et al. [33] through experimental research. The E-C interaction rate includes the changed amount of corrosion rate caused by erosion and the changed amount of erosion rate caused by corrosion, as shown in Fig. 12. It can be seen that the changed amount of corrosion rate caused by erosion and the changed amount of erosion rate caused by corrosion are both positive values, which indicates that mechanical erosion and electrochemical corrosion could contribute to each other, thus causing a significant increase in the E-C loss. In the E-C interaction rates, the changed amounts of corrosion rates caused by erosion are far greater than that of erosion rates caused by corrosion. The changed amounts of erosion rates caused by corrosion are between 0.43 and 2.46 mm/yr, while that of corrosion rates caused by erosion are between 2.54 and 7.46 mm/yr. In the E-C rate, the percentages of the changed amounts of erosion rates caused by corrosion are between 9.3% and 28.0%, while that of the changed amounts of corrosion rates caused by erosion are between 63.2% and 84.9%. Therefore, in the E-C process of liquid/solid two-phase flow, mechanical erosion is more important than electrochemical erosion, which indicates that mechanical erosion plays a dominant role, and electrochemical corrosion plays a subordinate role in E-C. The interaction between electrochemical corrosion and mechanical erosion is the main cause of damage to metal materials [34]. Tang et al. [35] found the contributions of corrosion and erosion to the E–C rate of X-65 pipe steel in oil–sand slurry was approximately 30% and 70%, and erosion dominated the E–C of X-65 steel in oil–sand slurry through an impingement jet system.

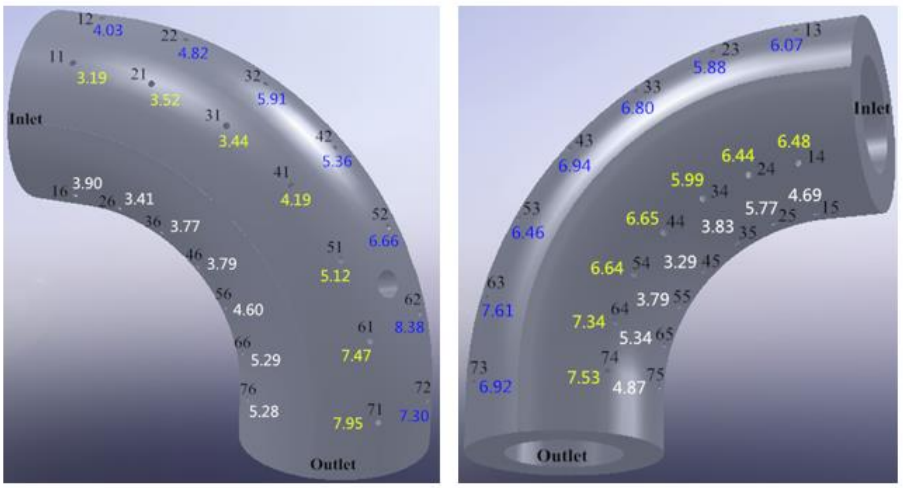

Figure 11. Interaction rates of E-C at different locations of the elbow

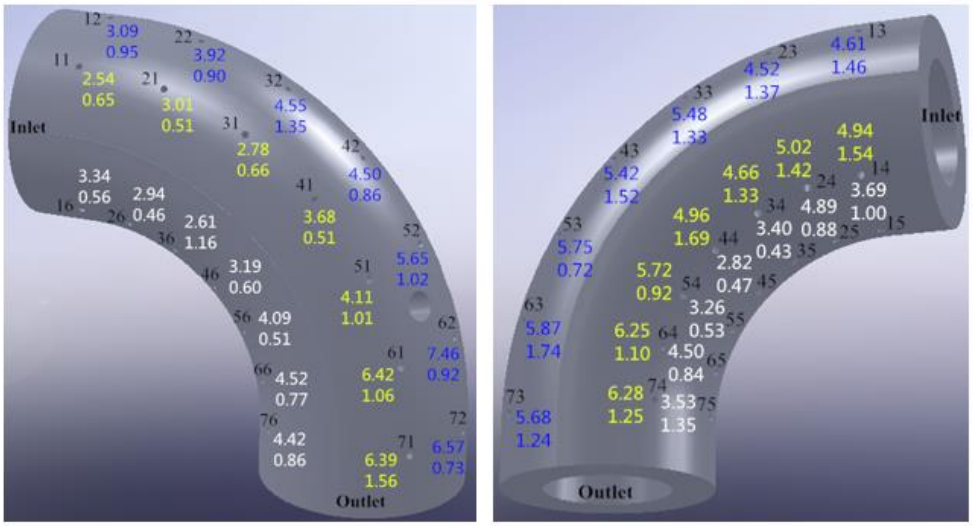

Figure 12. The changed amounts of the corrosion rates caused by erosion and the changed amounts of the erosion rates caused by corrosion at different locations of the elbow

3.3 Surface analysis

3.3.1 Macroscopic corrosion morphologies

The E-C morphologies of specimens at axial angle θ=45° of the elbow after E-C experiment are shown in Fig. 13. The surfaces of the specimens are covered with a layer of yellow-brown products. There are obvious E-C traces on the surfaces of specimens, and the local matrix is flaked off, forming E-C pits and grooves. Besides, there are differences in the sizes and depths of these grooves on the surfaces of specimens at different locations of the elbow, namely that the E-C is also different at different locations of the elbow, which is consistent with weight loss measurements. The formation of pits and grooves is the result of interaction between mechanical erosion and electrochemical corrosion

of the medium under the condition of liquid/solid two-phase flow, mechanical erosion continuously exposes the fresh metal matrix in the medium, the exposed fresh matrix produces electrochemical corrosion, and mechanical erosion continuously causes corrosion products to fall off, in this way, it enters a vicious cycle process, as a result, the depths of corrosion pits and grooves continue to deepen and the area continues to increase, the E-C rates of metal materials are greatly intensified, which eventually leads to equipment failure and even major safety accidents.

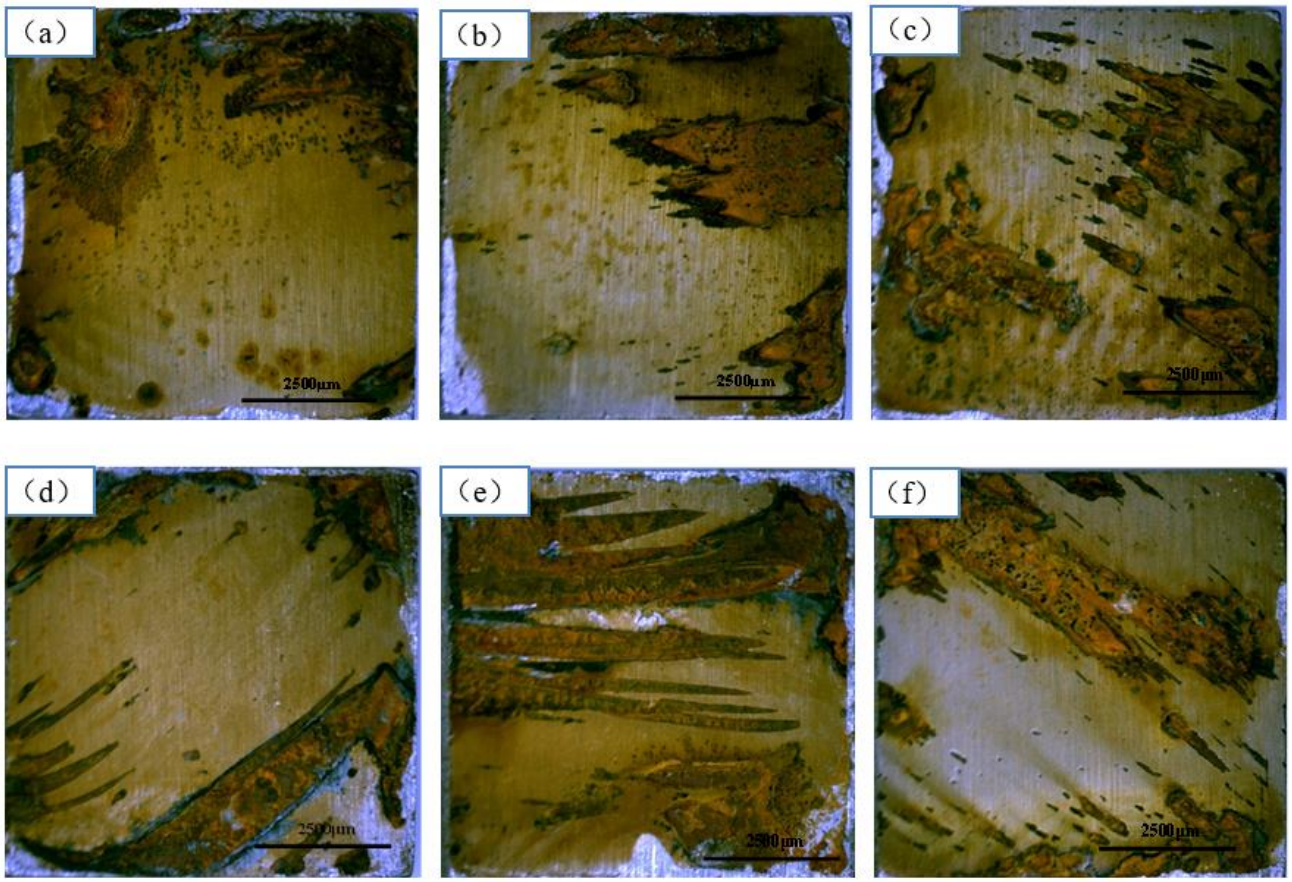

Figure 13. E-C morphologies of specimens at the axial angle of θ=45° of the elbow after the E-C experiment: (a) 41, (b) 42, (c) 43, (d) 46, (e) 45 and (f) 44

3.3.2 3D corrosion morphologies

Fig. 14 presents the 2D and 3D morphologies of typical specimens (No. 32, and 64) at the elbow. It can be seen that the morphologies of these specimen surfaces are mainly pits and grooves, with small depths, vertical edges, and uneven bottoms. The range of the maximum pit depths at different locations of the elbow is between 105.9 and 200.4μm. In addition, there are differences in the maximum pit depths on the surfaces of specimens at different locations of the elbow. Due to the different erosion angles of solution at different locations of the elbow, the erosion and impact on the surfaces of specimens are also different at different locations of the elbow.

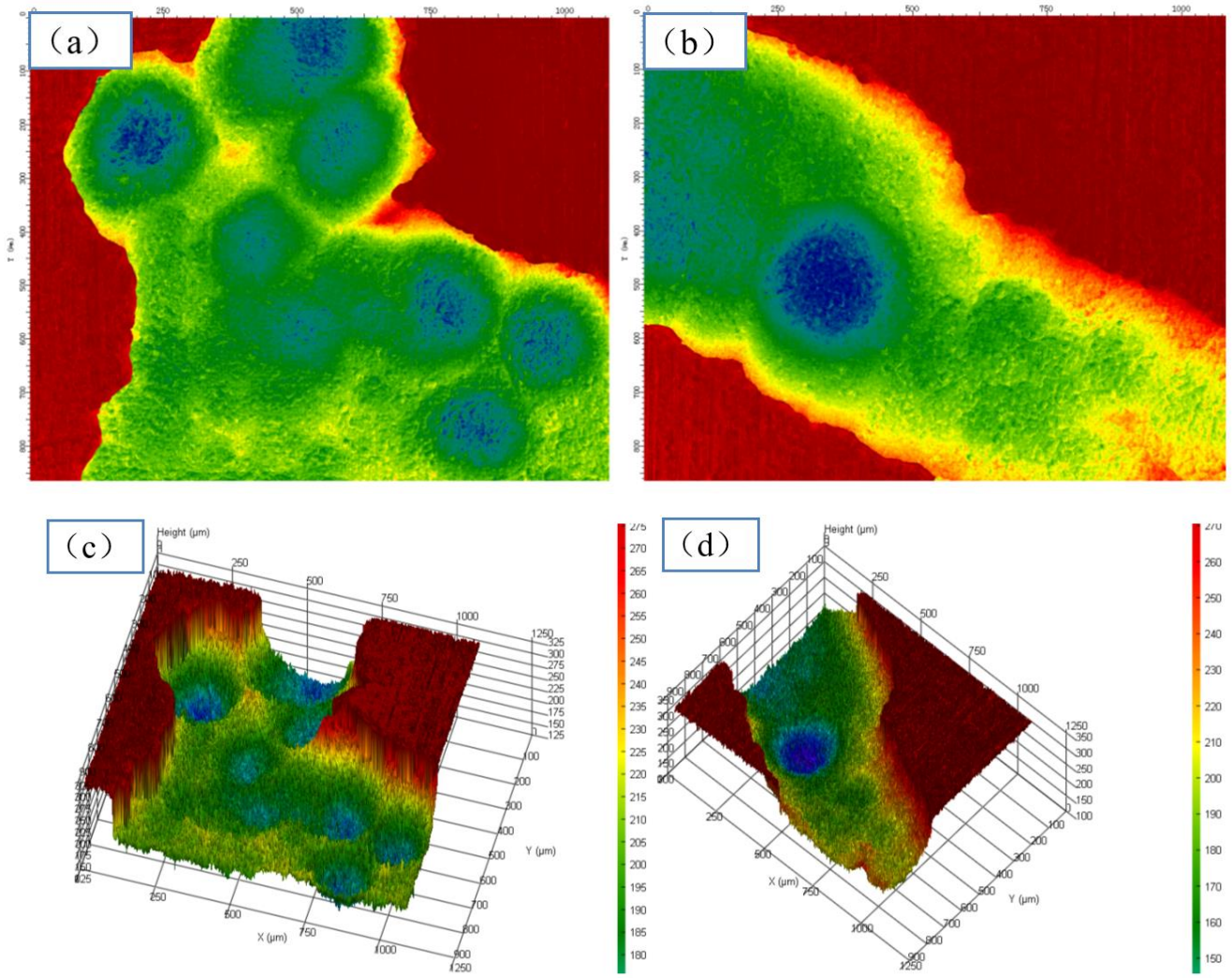

Figure 14. 2D and 3D morphologies of typical specimens at the elbow: (a) 2D morphology of 32, (b) 2D morphology of 64, 3D morphology of 32 and 3D morphology of 64

4. CONCLUSIONS

The total E-C rates are quantified through a loop experimental device. There are differences in the total E-C rates of different locations of a 90° horizontal elbow, between 3.49 and 8.81 mm/yr. Besides, the areas with severe E-C appear at the bottom of the elbow and the outer part of the elbow outlet.

The four components of the E-C rate and their percentages in the E-C rate at different locations of the elbow are quantified by the weight loss measurements and electrochemical measurements. Under the condition of liquid/solid two-phase flow, the pure corrosion rates and pure erosion rates are small at different locations of the elbow, and their percentages in the E-C rates are also small. However, the E-C interaction rates are very large, and their percentages in the E-C rates are also very large. Therefore, the interaction between electrochemical corrosion and mechanical erosion is the dominant cause of damage to metal materials.

In the E-C interaction rate, the changed amounts of corrosion rates caused by erosion and the changed amounts of erosion rates caused by corrosion are both positive values, which demonstrates that mechanical erosion and electrochemical corrosion can contribute to each other, with the former playing a dominant role and the latter playing a subordinate role.

There are differences in the flow characteristics and E-C morphologies at different locations of the elbow. The macroscopic E-C morphologies are mainly presented as pits and grooves, and the grooves have obvious directionality. The maximum pit depths are between 105.9 and 200.4μm at different locations of the elbow.

ACKNOWLEDGEMENTS
This work was supported by the Shandong Provincial Natural Science Foundation, China (ZR2019MEM014) and the Gansu Province Youth Science and Technology Fund project, China (20JR10RA571).

References

1. Z.B. Zheng, Y.G. Zheng, X. Zhou, S.Y. He, W. H. Sun, J. Q. W, *Corros. Sci.*, 88 (2014) 187.
2. J. Aguirre, M. Walczak, M. Rohwerder, *Wear*, 438–439 (2019) 203053.
3. M. M. Stack, N. Corlett, S.Turgoose, *Wear,* 255 (2003) 225.
4. H. Shahali, H. M. Ghasemi, M.Abedini, *Mater. Chem. Phys*., 233 (2019) 366.
5. X. M. Hu, A. Neville, *Wear*, 267 (2009) 2027.
6. D. López, N. A. Falleiros, A. P. Tschiptschin, *Tribol. Int*., 44 (2011) 610.
7. L. Cui, Z. Li, Y.H. Dou, J Fail, *Anal. Preven*., 18 (2018) 640.
8. H. Meng, X. Hu, A.Neville, *Wear*, 263 (2007) 355.
9. G. A. Zhang, Y. F. Cheng, *Corros. Sci*., 52(2010) 2716.
10. O. M. Irfan, *Int. J. Electrochem. Sci*., 16 (2021).
11. F. Mohammadi, J. Luo, *Corros. Sci*., 52 (2010) 2994.
12. Y. Yang, Y. F. Cheng, *Wear*, 276 /277 (2012) 141.
13. M. M. Stack, T. M. A. El Badia, *Surf. Coat. Technol*., 201 (2006) 1335.
14. M. El-Gammala, H. Mazhara, J. S. Cotton, C. Shefski, J. Pietralik, C. Y. Ching, *Nucl. Eng. Des*., 240 (2010) 1589.
15. R. Elemuren, R. Evitts, I. Oguocha, G. Kennell, R. Gerspacher, A. Odeshi, *Wear*, 410(2018)149.
16. W. M. Ma, J. H. Wang, Q. S. Li, D. H. Xia, W. B. Hu, *Int. J. Electrochem. Sci*, 14 (2019) 2560.
17. M. M. Stack, S. M. Abdelrahman, *Wear,* 273 (2011) 38.
18. A. Okhovat, S. Z. Heris, M. A. Haj Asgarkhani, ·K. Mohamadi Fard, *Arabian J. Sci. Eng*., 39 (2007) 1497.
19. J. G. Liu, W. L. BaKeDaShi, Z. L. Li, Y. Z. Xu, W. R. Ji, C. Zhang, G. Cui, R.Y. Zhang, *Wear*, 376 (2017) 526.
20. R. Malka, S. Nešić, D. A. Gulino, *Wear*, 262 (2007) 791.
21. M. A. Islam, Z. N.Farhat, *Tribol. Int*., 68 (2013) 26.
22. H. X. Guo, B. T. Lu, J. L. Luo, *Electrochim. Acta*, 51 (2005) 315.
23. O.O. Ige, S. Aribo, B. A.Obadele, T. Langa, P.A. Olubambi, *Tribol. Int*., 109 (2017) 441.
24. 24.M. Abedini, H. M. Ghasemi, *Wear,* 319(2014)49.
25. 25.J. Feyerl, G. Mori, S. Holzleitner, J. Haberl, M. Oberndorfer, W. Havlik, C. Monetti, *Corros.*, 64 (2008) 175.
26. 26. R.J. Chung a, J. Jiang, C. Pang, B. Yu, R. Eadie, D.Y. Li, *Wear*, 477 (2021) 203771.

27. 27. F. N. Sun, R. Z. Xie, B. He, Z. W. Chen, X. L. Bai, P. J. Han, *Int. J. Electrochem. Sci*., 16 (2021) 150878.
28. 28. J. B. Liu, J. H. Wang, W. B. Hu, *Int. J. Electrochem. Sci*., 14 (2019) 262.
29. 29. W. S. Peng, X. W. Cao, *Powder Technol*., 294 (2016) 266.
30. 30. W.S. Peng, X. W. Cao, J. Hou a, K. Xu, Y. Fan, S. H. Xing, *J. Nat. Gas Sci. Eng*., 76 (2020) 103175.
31. 31. S. Zhou, M.M. Stack, R.C. Newman, *Corros. Sci*., 38 (1996) 1071.
32. 32. B.R. Tian, Y.F. Cheng, *Corros. Sci*., 50 (2008) 773.
33. 33. L. Zeng, G.A. Zhang, X.P. Guo, *Corros. Sci*., 85 (2014) 318.
34. 34. Y. F. Liu, Y. L. Zhao, J. Yao, *Wear*, 466 (2021) 203572.
35. 35. X. Tang, L. Y. Xu, Y. F. Cheng, *Corros. Sci*., 50 (2008) 1469.